



Published in final edited form as:

*Mod Pathol.* 2021 February ; 34(2): 264–279. doi:10.1038/s41379-020-00659-9.

## Subependymal giant cell astrocytomas are characterized by mTORC1 hyperactivation, a very low somatic mutation rate, and a unique gene expression profile

Krinio Giannikou<sup>1,2</sup>, Zachary Zhu<sup>1</sup>, Jaegil Kim<sup>2</sup>, Kellen D. Winden<sup>3</sup>, Magdalena E. Tyburczy<sup>1</sup>, David Marron<sup>4</sup>, Joel S. Parker<sup>4</sup>, Zachary Hebert<sup>5</sup>, Anika Bongaarts<sup>6</sup>, Len Taing<sup>7</sup>, Henry W. Long<sup>7</sup>, William V. Pisano<sup>8</sup>, Sanda Alexandrescu<sup>9</sup>, Brianna Godlewski<sup>3</sup>, Mark Nellist<sup>10</sup>, Katarzyna Kotulska<sup>11</sup>, Sergiusz Jozwiak<sup>11</sup>, Marcin Roszkowski<sup>12</sup>, Marek Mandra<sup>13</sup>, Elizabeth A. Thiele<sup>14</sup>, Hart Lidov<sup>9</sup>, Gad Getz<sup>2</sup>, Orrin Devinsky<sup>15</sup>, Michael S. Lawrence<sup>16</sup>, Keith L. Ligon<sup>8</sup>, David W. Ellison<sup>17</sup>, Mustafa Sahin<sup>3</sup>, Eleonora Aronica<sup>6,18</sup>, David M. Meredith<sup>19</sup>, David J. Kwiatkowski<sup>1,2</sup>

<sup>1</sup>Cancer Genetics Laboratory, Division of Pulmonary and Critical Care Medicine, Brigham and Women's Hospital and Harvard Medical School, Boston, MA, USA

<sup>2</sup>Broad Institute of MIT and Harvard, Cancer Genome Program, Cambridge, MA, USA

<sup>3</sup>Department of Neurology, Boston Children's Hospital, Harvard Medical School, Boston, MA, USA

<sup>4</sup>Lineberger Comprehensive Cancer Center, The University of North Carolina at Chapel Hill, Chapel Hill, NC, USA

<sup>5</sup>Molecular Biology Core Facility, Dana Farber Cancer Institute, Boston, MA, USA

<sup>6</sup>Amsterdam UMC, University of Amsterdam, Department of (Neuro)Pathology, Amsterdam Neuroscience, Amsterdam, the Netherlands

<sup>7</sup>Center for Functional Cancer Epigenetics, Department of Medical Oncology, Dana-Farber Cancer Institute and Harvard Medical School, Boston, MA, USA

<sup>8</sup>Department of Oncologic Pathology, Dana-Farber Cancer Institute, Boston, MA, USA

<sup>9</sup>Department of Pathology, Boston Children's Hospital, Harvard Medical School, Boston, MA, USA

<sup>10</sup>Department of Clinical Genetics, Erasmus Medical Centre, Rotterdam, The Netherlands

<sup>11</sup>Department of Child Neurology, Medical University of Warsaw, Warsaw, Poland

<sup>✉</sup>Krinio Giannikou, kgiannikou@bwh.harvard.edu; David J. Kwiatkowski, dk@rics.bwh.harvard.edu.

**Author contributions** KG: conceptualized the study, performed experiments, analyzed and interpreted high throughput data, wrote and submitted the paper for publication. ZZ, JK, KDW, MET, DM, JSP, ZH, LT, HL, GG, and MSL: executed experiments or/and performed high throughput analyses. AB, WP, BG, MN, MM, and EA: contributed material; SA: selected a subset of the pediatric cases, evaluated their histology, and provided biospecimens. KK, SJ, MR, EAT, MM, HL, OD, KLL, DWE, MS, and EA: evaluated the patients/biospecimens or/and provided clinical data. DMM: provided biospecimens, performed pathology analysis of the tumors and contributed to experimental design; DJK: conceptualized and supervised the study, reviewed and interpreted data and contribute to paper preparation. All authors read and commented on the paper.

**Conflict of interest** The authors declare that they have no conflict of interest.

**Supplementary information** The online version of this article (<https://doi.org/10.1038/s41379-020-00659-9>) contains supplementary material, which is available to authorized users.

<sup>12</sup>Department of Neurosurgery, The Children's Memorial Health Institute, Warsaw, Poland

<sup>13</sup>Department of Pediatric Neurosurgery, Medical University of Silesia, Katowice, Poland

<sup>14</sup>Department of Neurology, Massachusetts General Hospital, Boston, MA, USA

<sup>15</sup>Department of Neurology, New York University School of Medicine, 223 E 34 Street, New York, NY, USA

<sup>16</sup>Broad Institute of MIT and Harvard, Massachusetts General Hospital Cancer Center, Department of Pathology, Harvard Medical School, Charlestown, MA, USA

<sup>17</sup>Department of Pathology, St. Jude Children's Research Hospital, Memphis, TN, USA

<sup>18</sup>Stichting Epilepsie Instellingen Nederland (SEIN), Zwolle, The Netherlands

<sup>19</sup>Department of Pathology, Brigham and Women's Hospital, Harvard Medical School, Boston, MA, USA

## Abstract

Subependymal giant-cell astrocytomas (SEGAs) are slow-growing brain tumors that are a hallmark feature seen in 5–10% of patients with Tuberous Sclerosis Complex (TSC). Though histologically benign, they can cause serious neurologic symptoms, leading to death if untreated. SEGAs consistently show biallelic loss of *TSC1* or *TSC2*. Herein, we aimed to define other somatic events beyond *TSC1/TSC2* loss and identify potential transcriptional drivers that contribute to SEGA formation. Paired tumor-normal whole-exome sequencing was performed on 21 resected SEGAs from 20 TSC patients. Pathogenic variants in *TSC1/TSC2* were identified in 19/21 (90%) SEGAs. Copy neutral loss of heterozygosity (size range: 2.2–46 Mb) was seen in 76% (16/21) of SEGAs (44% chr9q and 56% chr16p). An average of 1.4 other somatic variants (range 0–7) per tumor were identified, unlikely of pathogenic significance. Whole transcriptome RNA-sequencing analyses revealed 190 common differentially expressed genes in SEGA ( $n = 16$ , 13 from a prior study) in pairwise comparison to each of: low grade diffuse gliomas ( $n = 530$ ) and glioblastoma ( $n = 171$ ) from The Cancer Genome Atlas (TCGA) consortium, ganglioglioma ( $n = 10$ ), TSC cortical tubers ( $n = 15$ ), and multiple normal tissues. Among these, homeobox transcription factors (TFs) *HMX3*, *HMX2*, *VAX1*, *SIX3*; and TFs *IRF6* and *EOMES* were all expressed >12-fold higher in SEGAs (FDR/ $q$ -value < 0.05). Immunohistochemistry supported the specificity of IRF6, VAX1, SIX3 for SEGAs in comparison to other tumor entities and normal brain. We conclude that SEGAs have an extremely low somatic mutation rate, suggesting that *TSC1/TSC2* loss is sufficient to drive tumor growth. The unique and highly expressed SEGA-specific TFs likely reflect the neuroepithelial cell of origin, and may also contribute to the transcriptional and epigenetic state that enables SEGA growth following two-hit loss of *TSC1* or *TSC2* and mTORC1 activation.

---

## Introduction

Subependymal giant cell astrocytomas (SEGAs) are slow growing, glioneuronal brain neoplasms that represent 2% of all pediatric brain tumors. SEGAs are seen almost exclusively in patients with tuberous sclerosis complex (TSC, MIM# 191100, 191092).

Approximately, 5–10% of patients with TSC develop SEGAs, of which nearly all are diagnosed in childhood [1–4]. TSC is a multisystem neurocutaneous genetic syndrome that affects multiple organ systems, including the central nervous system (CNS) with cortical tubers, white matter heterotopias, subependymal nodules (SENs), and SEGAs [3, 4]. SEGAs have been shown to have either *TSC1* or *TSC2* biallelic inactivation in about 80% of cases, following the classic Knudson two hit model, leading to complete loss of function of the tuberin-hamartin protein complex and mTORC1 (mechanistic Target Of Rapamycin Complex 1) hyperactivation [1, 5, 6]. Other genetic aberrations, including partial loss of chr22 and *BRAFV600E* mutation have been reported in a few cases [7, 8].

SEGAs develop from benign, smaller, histologically similar lesions, known as subependymal nodules (SEN), near the foramen of Monro. Although SEGAs are benign histologically, they can cause serious neurological complications, including obstructive hydrocephalus, intractable seizures, and if left untreated can lead to death. Clinical diagnosis is based on neuroimaging of TSC patients where SEGAs are defined as having maximum diameter  $\geq 10$ mm and/or growth seen on serial scans [2]. There are occasional patients in whom SEGAs-like lesions are seen and other features of TSC are not prominent, as well as TSC patients in whom the SEGAs location is atypical. Histologically, SEGAs consist of large cells resembling gemistocytic astrocytes that are arranged in fascicles, sheets and nests; the tumor cells show variable expression of glial and neuronal markers, with high levels of cytoplasmic phospho-S6K, phospho-S6, and phospho-Stat3, proteins downstream of mTORC1 [1, 5].

Treatment options for SEGAs include mTORC1 allosteric inhibitors, rapamycin (sirolimus) and everolimus, termed rapalogs, as well as surgical resection. However, resection is challenging due to their deep intracranial location. On the other hand, continuous rapalog treatment is required as tumors can regrow when rapalog therapy is discontinued [2, 9–11].

The evidence that additional genetic events beyond *TSC1/TSC2* biallelic inactivation lead to SEGAs formation has been limited to date [5, 6]. Previous studies have shown that SEGAs have a distinct gene expression profile compared to periventricular normal brain [7, 12, 13]. However, a comparison to other brain tumors has not been performed previously and several questions remain regarding the pathogenic mechanisms involved in SEGAs.

Herein, we aimed to define the prevalence of other somatic genetic events that might contribute to SEGAs formation in a large series of resected SEGAs tumors. In addition, we identified differentially expressed genes (DEGs) in SEGAs in comparison to a broad panel of CNS tumors and cortical tubers, in order to provide insight as to their cell of origin, unravel novel aspects of their tumor biology, as well as to identify potential transcriptional driver events for SEGAs.

## Materials and methods

### Patient recruitment and tumor collection

This study was conducted in compliance with Partners Human Research Committee Institutional Review Board Approval (2011P002651) at the Brigham and Women's Hospital

and in compliance with the Office of Human Research Studies (DF/HCC 10-417) at the Dana Farber Cancer Institute. Signed informed consent or waiver of consent was obtained from patients and/or their guardians, and the sample collection and usage was in accordance with the policies of the institutional review boards at the respective institutions. All samples were de-identified for analysis; we followed the Declaration of Helsinki (World Medical Association Declaration of Helsinki, 2013. <https://doi.org/10.1001/jama.2013.281053>). The inclusion criteria in the present study were diagnosis of SEGAs, confirmed by histopathological assessment accordingly to the 2016 WHO classification for CNS tumors (Fig. 1a, b) by experienced neuropathologists, and a definite clinical diagnosis of TSC based on current criteria [14–17].

Fresh-frozen surgically resected tumor specimen and/or formalin-fixed paraffin-embedded (FFPE) samples ( $n = 21$ ) and matching peripheral blood as normal control for comparison were obtained from 20 patients with TSC (male  $n = 10$ , female  $n = 10$ , age range: 1–47, median = 13.5 years), for exome sequencing analysis. Clinicopathological data were available for all cases (Table 1).

### Histopathology studies

Conventional hematoxylin and eosin (H&E) staining was performed. The tumor-cell content was estimated to be at least 80% in all SEGA cases by H&E staining, except for one case (SEGA-S19) in which tumor purity was reduced due to the contamination with non-tumor and inflammatory cells. Immunohistochemistry (IHC) was performed on 5-micron tissue sections as described previously [6, 18]. Antibodies against the following proteins were used for IHC: **MAP2** (mouse clone HM2, Sigma 1:100), **HLA-DR** (mouse clone CR3/43, DAKO, 1:100), **CD3** (mouse monoclonal, clone F7.2.38, DAKO; 1:200), **pS6** (rabbit polyclonal, Cell Signaling Technology, 1:50), **GFAP** (rabbit polyclonal, DAKO, 1:4,000), **Vimentin** (mouse clone V9, DAKO, 1:1,000), **NeuN** (mouse clone MAB377, Chemicon, 1:2,000); **IRF6** (mouse monoclonal, Origene, Cat. No. UM500074, 1:500); **SIX3** (rabbit polyclonal, LSBio, Cat. No. LS-B9336–50, 1:4000); **VAX1** (mouse monoclonal, Origene, Cat. No. CF811439; 1:100). Information for additional IHC staining is included in Supplementary material.

### Exome sequencing methods

Exome hybrid capture, library preparation, massively parallel sequencing (MPS), and bioinformatic analyses were performed at the Broad Institute of MIT and Harvard, following standard methods. Briefly, genomic DNA was sheared in a Covaris sonicator (Covaris, Woburn, MA, USA) to fragments of 200–500 bp, and subject to capture using the MPS Illumina Exome (37.7 Mb of mainly exonic territory; Agilent SureSelect All Exon V2) [19, 20]. Pooled indexed libraries were sequenced on either the HiSeq 2000 or HiSeq 2500 instrument (Illumina platform), using 76 bp paired-end sequencing. The mean coverage for the targeted region was 105x (range: 49–267x) for all tumors and 113x (range: 47–192x) for normal samples. An average of 76% in the targeted region (range: 46–93%) was covered at 50x for tumor, whereas it was 92% at 50x (range: 80–95%) for normal.

## Pre-processing and bioinformatics analysis of MPS data

Demultiplexing/sample deconvolution, base alignment and sequence quality control were performed using Picard tools and the Firehose pipeline at the Broad Institute of MIT and Harvard. Fastq files were generated and unique reads were aligned to the human reference genome GRCh37(hg19) using BWA (v0.7.3a) [<http://arxiv.org/abs/1303.3997>] and Bowtie 2 (<http://bowtie-bio.sourceforge.net/bowtie2/index.shtml>). Variant calling for single nucleotide variants (SNVs) and insertion/deletions (indels) was performed using Haplotype Caller in Genome Analysis Toolkit (GATK, v3.0) Best Practices. Sequencing data were then analyzed using the Cancer Genome Analysis pipeline, as well as custom code in Python, Matlab and Unix to enable the detection of *TSC1/TSC2* deleterious sequence variants with low mutant allele frequency (MAF) [5]. Somatic point mutations were called by MuTect (<http://www.broadinstitute.org/cancer/cga/mutect/>) and short insertions and deletions in sequencing data were identified by SomaticIndelDetector. All variants were annotated using Oncotator (<http://www.broadinstitute.org/oncotator>). We used ABSOLUTE to estimate tumor purity, tumor cell ploidy, and to determine chromosomal copy-numbers genome-wide [21]. All somatic variant calls were reviewed manually using IGV (<https://software.broadinstitute.org/software/igv/>), and those reflecting sequencing or other artifacts were excluded. Variant nomenclature was confirmed by Mutalyzer (<https://mutalyzer.nl/>). SIFT and PROVEAN *in silico* prediction tools (<http://provean.jcvi.org/index.php>) were used to assess the functional effects of missense variants. Called variants were validated by either Sanger sequencing (variants with MAF > 10%) or amplicon MPS method (variants with MAF < 10%) for 10 out of 21 SEGAs with DNA material available [22, 23].

## Whole transcriptome RNA sequencing

Paired end RNA-sequencing (RNA-seq) was performed on 3 SEGA tumors (**SEGA-S3, S4, S19** with matching exome data) at the Broad Institute of MIT and Harvard, following standard methods (Illumina platform). Additional RNA-seq raw data were obtained from 13 SEGAs from a previous study [6] and were reanalyzed for uniformity and downstream analyses. After quality assessment and filtering for all SEGA tumors, raw reads were mapped or aligned to the reference genome GRCh37 (hg19) build using the STAR program [24]. VIPER (Visualization Pipeline for RNA-seq analysis) [25] QC analysis for all combined 16 SEGAs revealed high quality sequencing data with a median of ~25 million paired end reads generated for each tumor (range: 21–97M reads). FPKM normalized values for all genes and their isoforms were generated using Cufflinks v2.2.1. Raw data were also converted into RSEM format for comparison to other brain and adult solid tumors from The Cancer Genome Atlas (TCGA) consortium and 10 gangliogliomas [26–29]. We also performed gene fusion analysis to identify any gene rearrangements using FusionInspector (<https://github.com/FusionInspector/FusionInspector/>), as a previous study reported a single SEGA case with PRRC2B-ALK fusion [30].

## Statistical analysis

Statistical analyses were performed using the non-parametric Mann–Whitney *U*-test in GraphPad Prism software (Graphpad Software Inc., La Jolla, CA). All *p*-values were corrected applying the Benjamini–Hochberg method. An adjusted *p*-value/FDR < 0.05 was

considered statistically significant. The following convention was used in all figures: \* $p$  0.05; \*\* $p$  0.01; \*\*\* $p$  0.001; \*\*\*\* $p$  0.0001.

## Results

### Clinical and routine diagnostic studies

In this study, we evaluated 21 SEGAs from 20 patients with TSC. Pre-operative brain MRIs demonstrated that these tumors were present on the medial or lateral ventricular wall, which is typical for these lesions (Fig. 1a and Table 1). H&E staining showed classic histologic features for SEGAs, featuring plump cells with abundant glassy eosinophilic cytoplasm and enlarged nuclei with distinct nucleoli (Fig. 1b). IHC showed variable expression of GFAP, MAP2, and HLA-DR; with consistent labeling for pS6, a marker of mTORC1 activation; and variable numbers of CD3+ cells (Fig. 1b).

### TSC1/TSC2 mutation analysis of SEGAs

Twenty-one paired SEGA-normal samples were analyzed by exome sequencing. *TSC1* and *TSC2* germline pathogenic variants were identified in 18 of 20 (90%) patients (6 *TSC1* mutations and 12 *TSC2* mutations) and were similar to the known pathogenic variant spectrum for these genes (Fig. 2a and Table S1; SEGA-S15 had a large *TSC1* deletion, as indicated by focal reduction in read depth for exons 18–23) [4]. Copy neutral loss of heterozygosity (CN-LOH) was seen in the *TSC2* region of chr16p in 9 of 12 (82%) tumors from subjects with pathogenic *TSC2* variants; size range: 2.2–30.3 Mb (Fig. 2b, Fig. S1 and Table S1). CN-LOH was also seen in chr9q encompassing *TSC1* in 6 SEGA tumors from subjects with pathogenic *TSC1* variants; size range: 6.7–46 Mb (Fig. 2b, Fig. S1 and Table S1). One tumor from one subject (**SEGA-S17**), with no germline mutation identified in either *TSC1* or *TSC2*, had CN-LOH in chr16p, suggesting an occult germline mutation in *TSC2* (Table S1 and Fig. S1). CN-LOH regions had a variable size on both chromosome 9 and 16, likely reflecting random mitotic recombination events, as seen previously in TSC kidney angiomyolipoma [31].

### Exome sequence analysis

Exome sequencing revealed 30 somatic point variants/indels in 10 of 21 (45%) tumor-normal matched samples, with a range: 0–7 variants/tumor (overall median 0, average 1.4, Fig. 2c and Table S2). None of these 30 somatic variants occurred in the same gene in different samples and 20 of 30 (67%) were subclonal, determined by ABSOLUTE. Twenty-three of the 30 variants (77%) were missense changes, of which 15 (65%) were classified as likely deleterious/damaging by *in silico* prediction analysis. None of the genes with somatic alterations were known ‘cancer genes’ [32]. These results suggest that these variants were likely passenger events that do not contribute to SEGA formation. We did not observe any mutations in *BRAF* in this SEGA cohort (Table S2), similar to our findings in a previous SEGA cohort [5].

We then compared the somatic mutation rate that we observed in SEGAs from our internal cohort ( $n = 21$ ) including 16 tumors from a previous study [6], with rates that have been reported for a wide variety of other brain tumors (Fig. 2d and Table S3), as well

as other TCGA tumors (Fig. S2) [33]. SEGAs in our analysis showed a similar, though slightly lower, mutation burden (SNVs per Mb) to pediatric medulloblastoma and hindbrain ependymoma, and a substantially lower mutation burden than both pediatric and adult low-grade gliomas.

Copy number alteration (CNA) analysis revealed subclonal chromosomal gains and/or losses in 5/21 (24%) tumors at either the arm or whole chromosome level, including chr21 and chr22 loss; and chr5 and chr19p gain (Fig. 2e). These results are similar to those reported previously, in which CNAs were seen in 3/14 (21%) SEGAs for several chromosomes (1, 5, 7, 11, 12, 17, and 19) [6].

### Gene expression RNA-seq analyses

We analyzed RNA-seq data for 16 SEGA tumors (see “Materials and methods”) in comparison to the TCGA brain tumor cohort, including low grade gliomas (LGG;  $n = 530$ ) and TCGA adult glioblastomas (GBM;  $n = 171$ ), as well as cortical tubers ( $n = 15$ ), SEN ( $n = 2$ ), and normal brain samples ( $n = 11$ ) [6, 29]. This set of 16 SEGA tumors was relatively pure, as reflected by the mutant allele frequency of either *TSC1* or *TSC2* mutation for each (SEGA-S3, S4, S20 and Martin et al. 2017 [6]).

To discern the potential relationship between SEGA and the large panel of brain tumors studied by TCGA, we performed a *de novo* clustering analysis for 3060 most variable genes in the combined cohort ( $n = 745$ ) by consensus Bayesian non-negative matrix factorization, and identified four distinct clusters (Cluster 1–4 in Fig. 3a and Table S4) [34]. Of note, 15 of 16 SEGAs were co-clustered with most GBM samples (95%, 163 out of 171) and 20% of LGG samples (103 out of 530) in Cluster 3. The set of 103 LGG in cluster 3 included 60 astrocytomas, 15 oligoastrocytomas, 16 oligodendrogliomas, and 12 unclassified brain tumors. Note that we recognize that the oligoastrocytoma designation for a subset of gliomas is no longer used; we retain that term here to be consistent with nomenclature used in TCGA project. The single SEGA that was not in cluster 3 was from Martin et al. [6] and was grouped in Cluster 1 with normal brain, suggesting that it was highly contaminated with normal brain.

To discern genes whose expression was specifically altered in SEGAs, and might contribute to SEGA development, we performed DESeq2 analyses using normalized read counts (RSEM). Pair wise comparisons were made between the SEGAs and each of the histological subtypes of LGG and GBM in Cluster 3 ([www.qiluore.com](http://www.qiluore.com)) to identify gene expression differences (Fig. 3a, b) [29, 34, 35]. We identified several hundred genes that were differentially expressed between SEGAs and other tumors at a false discovery rate (FDR)/ $q$ -value  $< 0.05$  and  $p$ -value  $< 0.002$  (Fig. 3b, Fig. S3a–f and Tables S5–S9).

Analysis of multiple housekeeping genes (e.g., *GAPDH*, *LDHA*, *SDHA*, and *ABCF1*) across different tumor samples analyzed showed no significant differences in expression, confirming a lack of artifact or bias due to different sample sets, library preparation, and/or sequencing methods (Fig. S4). A set of 190 genes was found to be differentially expressed in SEGAs, all consistently in the same direction (either up or downregulated), in comparison to each of the other sample types (Fig. 3b, Table S10). One hundred fifty one of these 190

common DEGs were also differentially expressed in SEGAs in comparison to normal brain (46 upregulated, 105 downregulated; FDR < 0.05,  $|\log_2\text{fold change}| \geq 1$ ) (Table S10).

Since many TFs regulate cell lineage and act as drivers of cancer growth in different cancer types, we chose to focus our analysis on TFs with higher expression in SEGAs compared to these other entities. Fourteen of 190 DEGs were TFs, of which 8 were upregulated (Table 2 and Table S11), including *HMX3*, *HMX2*, *IRF6*, *SIX3*, *EOMES*, and *VAX1*, each with a median fold change  $\geq 12$  (Fig. 3c and Table 2). We also found that the expression of *HMX3*, *HMX2*, *SIX3*, and *VAX1* was much higher in SEGAs than any other TCGA cancer type (2463 tumors of 27 different histological types) and normal tissues {~8500 samples from 30 normal tissue types; the Gene and Tissue Expression (GTEx) project} (Figs. 4, 5) [36]. *IRF6* and *EOMES* were also highly expressed in SEGAs but were also seen at relatively high levels in some other cancer types and normal tissues (Figs. 4, 5). In addition, *SIX3* was relatively highly expressed in pituitary gland (Figs. 4, 5). *ZBTB20*, another TF, was highly expressed in SEGAs compared to all brain tumors and cortical tubers, except for gangliogliomas where it was also highly expressed. *ZBTB20* was also much more highly expressed in SEGAs than all normal tissues (Figs. S5, S6).

Considering other differentially expressed genes other than TFs, *HCRTR2* was the most highly expressed gene in SEGAs compared to all tumors and normal tissues (Figs. S5, S6). *HCRTR2* is a G-protein coupled receptor that binds the hypothalamic neuropeptides orexin A and orexin B and regulates sleep-wakefulness. Of note, a recent study reports that hypothalamic orexin and mTOR activation mediate sleep dysfunction in a mouse model of TSC [37]. *GPNMB* (Glycoprotein Nmb) was also a top DEG between SEGAs and other pathological entities (Table 2 and Figs. S5, S6). We had previously demonstrated that *GPNMB* was upregulated in *Tsc2* null neuroepithelial cells [38]. No gene fusion events in any of 16 SEGAs analyzed by RNA-Seq were identified.

### GSEA pathway enrichment analyses

To examine the biological pathways enriched in SEGAs, we performed Gene Set Enrichment Analysis (GSEA; <https://www.gsea-msigdb.org>) using all 190 common DEGs from above. Ten GO gene sets were enriched for DEGs that were downregulated in SEGAs (Fig. 3d; top; Table S12); while 8 were enriched for DEGs that were upregulated in SEGAs (Fig. 3d; bottom). The downregulated gene sets were associated with normal brain development, including GO\_synapse and GO\_synaptic signaling, indicating that even by comparison to these other brain tumors, SEGAs have less neuronal differentiation. In contrast, the upregulated gene sets were associated with morphogenesis, cell surface and WNT protein binding.

### Immunohistochemistry confirmation

To confirm that the top highly expressed TF in SEGAs, identified by RNA-seq, were also highly expressed at protein level, we performed IHC on SEGAs and multiple other pediatric and adult gliomas (Figs. 6–8) using commercially available antibodies. We stained at least 2–5 sections available per tumor type, including SEGAs, cortical tuber, adult glioblastoma, pleomorphic xanthoastrocytoma (PXA), diffuse



astrocytoma, oligodendroglioma, subependymoma, as well as normal brain (cortex) (detailed neuropathology evaluation for each stained marker in Table S13). Positivity was defined as moderate-to-strong nuclear or cytoplasmic immunoreactivity in at least 5–25% of cells.

IHC was attempted for each of the top six DE TFs, including *HMX3*, *HMX2*, *IRF6*, *SIX3*, *EOMES*, and *VAX1*, as well as *ZBTB20*. Antibodies for *HMX3* and *HMX2* failed to give a reliable signal in SEGAs or any other tissue examined. Both *IRF6* and *SIX3* showed strong cytoplasmic immunoreactivity in nearly all SEGAs examined (3 of 3, 4 of 5, respectively), and no appreciable staining in other tumors types (Figs. 6, 7). *IRF6* and *SIX3* expression was also seen in the balloon cells of cortical tubers (2 of 3 samples examined). Both *VAX1* and *ZBTB20* showed strong nuclear immunoreactivity in all SEGAs (3 of 3 and 2 of 2, respectively). *VAX1* was highly specific for SEGAs, with little to no staining in other tumor types/lesions (Fig. 8), while *ZBTB20* showed moderate to high nuclear staining in all tumors and normal neurons Fig. S7. IHC for *EOMES* did not show specificity for SEGAs (data not shown).

IHC analysis also showed that *HCRTR2*, the gene with highest differential expression, showed cytoplasmic immunoreactivity in SEGAs and was not seen in other brain tumors/tubers apart from gangliogliomas (Fig. S7). *CTSK* (cathepsin K), a known marker for kidney angiomyolipoma, another benign tumor seen in the majority of TSC patients, showed very strong cytoplasmic staining in SEGAs (5 of 5, 100%). It was also seen in the balloon cells of cortical tubers (1 of 3, 33%) and in some glioblastoma (1 of 3, 33%) (Fig. S7). *GPNMB* showed very high expression in SEGAs and the balloon cells of cortical tubers but was not seen in normal cortex (Fig. S7).

### Unsupervised weighted gene co-expression network analysis (WGCNA)

We also performed unsupervised weighted gene co-expression network analysis (WGCNA), based on pairwise correlations for SEGAs versus TCGA low grade gliomas, glioblastomas, gangliogliomas, and cortical tubers in order to define modules (clusters of co-expressed genes) and intramodular hub genes enriched in SEGAs [39]. WGCNA identified 65 modules of correlating co-expressed genes, that contained 46–1701 genes (median: 102, average: 231). We then determined a correlation score for each module to SEGAs tumors, and assigned  $k_{ME}$  scores to each gene (Tables S14, S15, and Fig. S8). Genes with higher  $k_{ME}$  scores are considered “hub” genes that may regulate expression within that module. Module ME65, with 47 genes, had the highest correlation score, 0.84, and showed the most consistent difference between SEGAs and the other tumors/cortical tubers. Module ME65 contained 21 of the 190 (11%) common DEGs, including 4 of the 6 TFs showing the largest median expression fold-change; *HMX3*, *HMX2*, *IRF6*, and *SIX3*. These results suggest that expression of *HMX3*, *HMX2*, *IRF6*, and *SIX3* TFs may be co-regulated in a synergistic manner, and that those genes may be master TFs for SEGAs, and function as transcriptional drivers of SEGAs development. Overall, the 190 DEGs were found in 25 different modules, with module M65, M66, and M85 containing the highest number of co-expressed DEGs (21, 31, 39 genes, respectively).

## Discussion

The present study reports multiplatform genomic and expression analyses in a large series of SEGA tumors, with detailed comparison to other brain tumors, other solid tumors, and multiple normal tissues. Exome sequence analysis of 21 matched tumor-normal pairs revealed that the mutational landscape of SEGAs is characterized by consistent biallelic inactivation of either *TSC1* or *TSC2*. In contrast, other somatic mutations appear to be random occurrences, without any duplicate events in this dataset, and very likely do not contribute to SEGA development. The frequency of other somatic mutations (0.80 mutation/Mb) is lower than, but similar to, that seen in TSC-related kidney angiomyolipoma (range 0–12 mutations, 2.1 mutations/Mb;  $p = 0.016$ , unpaired Mann–Whitney  $t$ -test), as previously reported [31]. CN-LOH was the most common second hit (81%) event in this cohort of SEGAs, similar to our previous reports on both SEGAs and angiomyolipomas [6, 7, 31]. This extremely low somatic mutation rate in SEGAs is similar to a small set of pediatric brain tumors, including atypical teratoid/rhabdoid tumors, pituitary adenoma, and pediatric medulloblastoma [40–44]. Our exome results strongly suggest that biallelic loss of *TSC1* or *TSC2* is all that is required genetically for SEGA development.

RNA-seq analyses showed that SEGAs have a unique expression profile compared to other brain tumors, having somewhat more similarity to TCGA oligodendrogliomas and cortical tubers, and less to TCGA astrocytomas and gangliogliomas. Seven TFs, *HMX3*, *HMX2*, *IRF6*, *SIX3*, *EOMES*, *VAX1*, and *ZBTB20*, were highly and relatively uniquely expressed in SEGAs. Little is known about the function of several of these, including potential roles in neurodevelopment. *HMX3* and *HMX2* are related NKL homeobox transcription factors involved in specification of neuronal cell types and organ development [45, 46]. *SIX3* is a sine oculis homeobox TF with a role in eye development, that regulates the proliferation and differentiation of neural progenitor cells through activating transcription of *CCND1* and *CCND2* [47]. *ZBTB20* is also highly expressed uniquely in SEGAs, and is a transcriptional repressor with roles in neurogenesis, glucose homeostasis, and postnatal growth [48]. *IRF6* (Interferon regulatory factor 6) plays a role in regulating mammary epithelial cell proliferation, while specifically expressed in SEGAs in comparison to other brain tumors but is expressed in other cancers and normal tissues [49]. These top genes have been reported to be epigenetically regulated bearing histone modifications: H3K27 trimethylation (H3K27me3) mark in brain for *HMX2*, *HMX3*, *IRF6*; H3K4me2 and H3K27me3 in neural precursor cells (NPC) for *HMX2*, *HMX3*, and *VAX1* [50].

*VAX1*, *SIX3*, and *IRF6* were all shown to be relatively highly and specifically expressed in SEGAs, suggesting that they may be useful to distinguish SEGAs from histologic mimics, including other brain tumors. However, our efforts to confirm the high and specific expression of these TFs in SEGAs were hampered by the failure of commercially available antibodies against *HMX2* and *HMX3* in IHC, and failure of attempts at RNA in-situ hybridization for *HMX3*.

Further studies are warranted to assess the functional importance of each of these TFs in SEGA development. Nonetheless, the key TFs *HMX2*, *HMX3*, *VAX1*, *SIX3*, and *IRF6*

may be considered as potential targets for the treatment of SEGAs, independent of, or in combination with mTORC1 inhibitors.

In conclusion, SEGAs have an extremely low somatic mutation burden, apart from *TSC1/TSC2*, similar to other pediatric brain tumors. Biallelic loss of either *TSC1* or *TSC2* occurs most commonly due to co-occurrence of a germline small mutation and CN-LOH as a second event, fitting the classic Knudson two hit mechanism. Several TFs, identified by RNA-seq analyses, are highly and relatively uniquely expressed in SEGAs. We consider that these TFs likely reflect the unique developmental state of the neuroepithelial cell in which biallelic loss of *TSC1/TSC2* gives rise to SEGAs. They may also be transcriptional drivers of SEGA growth whose expression is required.

## Supplementary Material

Refer to Web version on PubMed Central for supplementary material.

## Acknowledgements

The authors thank all subjects who participated in this study; the clinicians who referred and evaluated the patients and the neurosurgeons who performed the surgical resections; as well as Karthik V. Karnik and Edward R. Kwiatkowski for their work on customized code for MPS analysis, as well as Yana Stackpole for assistance with Qlucore analysis; Stichting Kinderen Kankervrij; Stichting AMC Foundation; Stichting TSC Fonds (EA, AB).

## Funding

This work was supported by the Engles Family Fund for Research in TSC and LAM.

## Data availability

Access to data which are not available within the article and Supplementary material, can be provided by the authors upon request (direct contact to KG or DJK).

## References

1. Chan JA, Zhang H, Roberts PS, Jozwiak S, Wieslawa G, Lewin-Kowalik J, et al. Pathogenesis of tuberous sclerosis subependymal giant cell astrocytomas: biallelic inactivation of *TSC1* or *TSC2* leads to mTOR activation. *J Neuropathol Exp Neurol*. 2004;63:1236–42. [PubMed: 15624760]
2. Kotulska K, Borkowska J, Roszkowski M, Mandera M, Daszkiewicz P, Drabik K, et al. Surgical treatment of subependymal giant cell astrocytoma in tuberous sclerosis complex patients. *Pediatr Neurol*. 2014;50:307–12. [PubMed: 24507694]
3. Henske EP, Jozwiak S, Kingswood JC, Sampson JR, Thiele EA. Tuberous sclerosis complex. *Nat Rev Dis Prim*. 2016;2:16035. [PubMed: 27226234]
4. Salussolia CL, Klonowska K, Kwiatkowski DJ, Sahin M. Genetic etiologies, diagnosis, and treatment of tuberous sclerosis complex. *Annu Rev Genomics Hum Genet*. 2019;20:217–40. [PubMed: 31018109]
5. Bongaarts A, Giannikou K, Reinten RJ, Anink JJ, Mills JD, Jansen FE, et al. Subependymal giant cell astrocytomas in Tuberous sclerosis complex have consistent *TSC1/TSC2* biallelic inactivation, and no BRAF mutations. *Oncotarget*. 2017;8:95516–29. [PubMed: 29221145]
6. Martin KR, Zhou W, Bowman MJ, Shih J, Au KS, Dittenhafer-Reed KE, et al. The genomic landscape of tuberous sclerosis complex. *Nat Commun* 2017;8:15816. 10.1038/ncomms15816. [PubMed: 28643795]

7. Lee D, Cho YH, Kang SY, Yoon N, Sung CO, Suh YL. BRAF V600E mutations are frequent in dysembryoplastic neuroepithelial tumors and subependymal giant cell astrocytomas. *J Surg Oncol.* 2015;111:359–64. [PubMed: 25346165]
8. Debiec-Rychter M, Jesionek-Kupnicka D, Zakrzewski K, Liberski PP. Cytogenetic changes in two cases of subependymal giant-cell astrocytoma. *Cancer Genet Cytogenet.* 1999;109:29–33. [PubMed: 9973956]
9. Franz DN, Belousova E, Sparagana S, Bebin EM, Frost M, Kuperman R, et al. Everolimus for subependymal giant cell astrocytoma in patients with tuberous sclerosis complex: 2-year open-label extension of the randomised EXIST-1 study. *Lancet Oncol.* 2014;15:1513–2150. [PubMed: 25456370]
10. Franz DN, Agricola K, Mays M, Tudor C, Care MM, Holland-Bouley K, et al. Everolimus for subependymal giant cell astrocytoma: 5-year final analysis. *Ann Neurol.* 2015;78:929–38. [PubMed: 26381530]
11. Fogarasi A, De Waele L, Bartalini G, Jozwiak S, Laforgia N, Verhelst H, et al. EFFECTS: an expanded access program of everolimus for patients with subependymal giant cell astrocytoma associated with tuberous sclerosis complex. *BMC Neurol.* 2016;16:126. [PubMed: 27502586]
12. Tyburczy ME, Kotulska K, Pokarowski P, Mieczkowski J, Kucharska J, Grajkowska W, et al. Novel proteins regulated by mTOR in subependymal giant cell astrocytomas of patients with tuberous sclerosis complex and new therapeutic implications. *Am J Pathol.* 2010;176:1878–90. [PubMed: 20133820]
13. Bongaarts A, van Scheppingen J, Korotkov A, Mijnsbergen C, Anink JJ, Jansen FE, et al. The coding and non-coding transcriptional landscape of subependymal giant cell astrocytomas. *Brain.* 2020;143:131–49. [PubMed: 31834371]
14. Louis DN, Perry A, Reifenberger G, von Deimling A, Figarella-Branger D, Cavenee WK, et al. The 2016 World Health Organization classification of tumors of the central nervous system: a summary. *Acta Neuropathol.* 2016;131:803–20. [PubMed: 27157931]
15. Wen PY, Huse JT. 2016 World Health Organization classification of central nervous system tumors. *Contin (Minneapolis Minn).* 2017;23:1531–47.
16. Diamandis P, Aldape K. World Health Organization 2016 classification of central nervous system tumors. *Neurol Clin.* 2018;36:439–47. [PubMed: 30072064]
17. Northrup H, Krueger DA, International Tuberous Sclerosis Complex Consensus Group. Tuberous sclerosis complex diagnostic criteria update: recommendations of the 2012 International Tuberous Sclerosis Complex Consensus Conference. *Pediatr Neurol.* 2013;49:243–54. [PubMed: 24053982]
18. Kim W, Giannikou K, Dreier JR, Lee S, Tyburczy ME, Silverman EK, et al. A genome-wide association study implicates NR2F2 in lymphangioleiomyomatosis pathogenesis. *Eur Respir J.* 2019;53(6):1900329. 10.1183/13993003.00329-2019. pii [PubMed: 31000673]
19. Gnirke A, Melnikov A, Maguire J, Rogov P, LeProust EM, Brockman W, et al. Solution hybrid selection with ultra-long oligonucleotides for massively parallel targeted sequencing. *Nat Biotechnol.* 2009;27:182–9. [PubMed: 19182786]
20. Fisher S, Barry A, Abreu J, Minie B, Nolan J, Delorey TM, et al. A scalable, fully automated process for construction of sequence-ready human exome targeted capture libraries. *Genome Biol.* 2011;12:R1. [PubMed: 21205303]
21. Carter SL, Cibulskis K, Helman E, McKenna A, Shen H, Zack T, et al. Absolute quantification of somatic DNA alterations in human cancer. *Nat Biotechnol.* 2012;30:413–21. [PubMed: 22544022]
22. Tyburczy ME, Dies KA, Glass J, Camposano S, Chekaluk Y, Thorner AR, et al. Mosaic and intronic mutations in TSC1/TSC2 explain the majority of TSC patients with no mutation identified by conventional testing. *PLoS Genet.* 2015;11:e1005637. [PubMed: 26540169]
23. Giannikou K, Lasseter KD, Grevelink JM, Tyburczy ME, Dies KA, Zhu Z, et al. Low-level mosaicism in tuberous sclerosis complex: prevalence, clinical features, and risk of disease transmission. *Genet Med.* 2019;21:2639–43. [PubMed: 31160751]
24. Dobin A, Davis CA, Schlesinger F, Drenkow J, Zaleski C, Jha S, et al. STAR: ultrafast universal RNA-seq aligner. *Bioinformatics.* 2013;29:15–21. [PubMed: 23104886]

25. Cornwell M, Vangala M, Taing L, Hebert Z, Köster J, Li B, et al. VIPER: visualization pipeline for RNA-seq, a snakemake workflow for efficient and complete RNA-seq analysis. *BMC Bioinforma.* 2018;19:135.
26. Trapnell C, Roberts A, Goff L, Pertea G, Kim D, Kelley DR, et al. Differential gene and transcript expression analysis of RNA-seq experiments with TopHat and Cufflinks. *Nat Protoc.* 2012;7:562–78. [PubMed: 22383036]
27. Li B, Dewey CN. RSEM: accurate transcript quantification from RNA-Seq data with or without a reference genome. *BMC Bioinformatics.* 2011;12:323. 10.1186/1471-2105-12-323. [PubMed: 21816040]
28. Qaddoumi I, Orisme W, Wen J, Santiago T, Gupta K, Dalton JD, et al. Genetic alterations in uncommon low-grade neuroepithelial tumors: BRAF, FGFR1, and MYB mutations occur at high frequency and align with morphology. *Acta Neuropathol.* 2016;131:833–45. [PubMed: 26810070]
29. Ceccarelli M, Barthel FP, Malta TM, Sabetot TS, Salama SR, Murray BA, et al. Molecular profiling reveals biologically discrete subsets and pathways of progression in diffuse glioma. *Cell* 2016;164:550–63. [PubMed: 26824661]
30. Tsurubuchi T, Nakano Y, Hirato J, Yoshida A, Muroi A, Sakamoto N, et al. Subependymal giant cell astrocytoma harboring a PRRC2B-ALK fusion: a case report. *Pediatr Blood Cancer.* 2019;66:e27995. 10.1002/pbc.27995. [PubMed: 31502411]
31. Giannikou K, Malinowska IA, Pugh TJ, Yan R, Tseng YY, Oh C, et al. Whole exome sequencing identifies TSC1/TSC2 biallelic loss as the primary and sufficient driver event for renal angiomyolipoma development. *PLoS Genet.* 2016;12:e1006242. 5. [PubMed: 27494029]
32. Bailey MH, Tokheim C, Porta-Pardo E, Sengupta S, Bertrand D, Weerasinghe A, et al. Comprehensive characterization of cancer driver genes and mutations. *Cell* 2018;174:1034–5. [PubMed: 30096302]
33. Lawrence MS, Stojanov P, Polak P, Kryukov GV, Cibulskis K, Sivachenko A, et al. Mutational heterogeneity in cancer and the search for new cancer-associated genes. *Nature* 2013;499:214–8. [PubMed: 23770567]
34. Robertson AG, Kim J, Al-Ahmadie H, Bellmunt J, Guo G, Cherniack AD, et al. Comprehensive molecular characterization of muscle-invasive bladder. *Cancer Cell.* 2017;171:540–56.
35. Love MI, Huber W, Anders S. Moderated estimation of fold change and dispersion for RNA-seq data with DESeq2. *Genome Biol.* 2014;15:550. [PubMed: 25516281]
36. Lonsdale J, Thomas J, Salvatore M, Phillips R, Lo E, Shad S, et al. The Genotype-Tissue Expression (GTEx) project. *Nat Genet.* 2013;45:580–5. [PubMed: 23715323]
37. Zhang B, Guo D, Han L, Rensing N, Satoh A, Wong M. Hypothalamic orexin and mechanistic target of rapamycin activation mediate sleep dysfunction in a mouse model of Tuberous sclerosis complex. *Neurobiol Dis* 2020;134:104615. [PubMed: 31605778]
38. Onda H, Crino PB, Zhang H, Murphey RD, Rastelli L, Gould BE, et al. Tsc2 null murine neuroepithelial cells are a model for human tuber giant cells, and show activation of an mTOR pathway. *Mol Cell Neurosci.* 2002;21:561–74. [PubMed: 12504590]
39. Langfelder P, Horvath S. WGCNA: an R package for weighted correlation network analysis. *BMC Bioinformatics.* 2008;9:559. 10.1186/1471-2105-9-559. [PubMed: 19114008]
40. Bettegowda C, Agrawal N, Jiao Y, Wang Y, Wood LD, Rodriguez FJ, et al. Exomic sequencing of four rare central nervous system tumor types. *Oncotarget.* 2013;4:572–83. [PubMed: 23592488]
41. Cancer Genome Atlas Research Network. Comprehensive genomic characterization defines human glioblastoma genes and core pathways. *Nature.* 2008;455:1061–8. [PubMed: 18772890]
42. Kline CN, Joseph NM, Grenert JP, van Ziffle J, Talevich E, Onodera C, et al. Targeted next-generation sequencing of pediatric neuro-oncology patients improves diagnosis, identifies pathogenic germline mutations, and directs targeted therapy. *Neuro Oncol.* 2017;19:699–709. [PubMed: 28453743]
43. Correa DD, Satagopan J, Martin A, Braun E, Kryza-Lacombe M, Cheung K, et al. Genetic variants and cognitive functions in patients with brain tumors. *Neuro Oncol.* 2019;21:1297–309. [PubMed: 31123752]

44. Muskens IS, Zhang C, de Smith AJ, Biegel JA, Walsh KM, Wiemels JL. Germline genetic landscape of pediatric central nervous system tumors. *Neuro Oncol.* 2019;21:1376–88. [PubMed: 31247102]
45. Feng Y, Xu Q. Pivotal role of hmx2 and hmx3 in zebrafish inner ear and lateral line development. *Dev Biol.* 2010;339:507–18. [PubMed: 20043901]
46. Wang W, Grimmer JF, Van De Water TR, Lufkin T. Hmx2 and Hmx3 homeobox genes direct development of the murine inner ear and hypothalamus and can be functionally replaced by *Drosophila* Hmx. *Dev Cell.* 2004;7:439–53. [PubMed: 15363417]
47. Yu Z, Sun Y, She X, Wang Z, Chen S, Deng Z, et al. SIX3, a tumor suppressor, inhibits astrocytoma tumorigenesis by transcriptional repression of AURKA/B. *J Hematol Oncol.* 2017;10:115. 10.1186/s13045-017-0483-2. [PubMed: 28595628]
48. Xie Z, Ma X, Ji W, Zhou G, Lu Y, Xiang Z, et al. Zbtb20 is essential for the specification of CA1 field identity in the developing hippocampus. *Proc Natl Acad Sci USA.* 2010;10:6510–5.
49. Guo XM, Chen B, Lv JM, Lei Q, Pan YJ, Yang Q. Knockdown of IRF6 attenuates hydrogen dioxide-induced oxidative stress via inhibiting mitochondrial dysfunction in HT22 cells. *Cell Mol Neurobiol.* 2016;36:1077–86. 10.1007/s10571-015-0301-8. [PubMed: 26620051]
50. Kozlenkov A, Li J, Apontes P, Hurd Y, Byne WM, Koonin EV, et al. A unique role for DNA (hydroxy)methylation in epigenetic regulation of human inhibitory neurons. *Sci Adv.* 2018;4:eaau6190. 10.n26/sciadv.aau6190..26. [PubMed: 30263963]

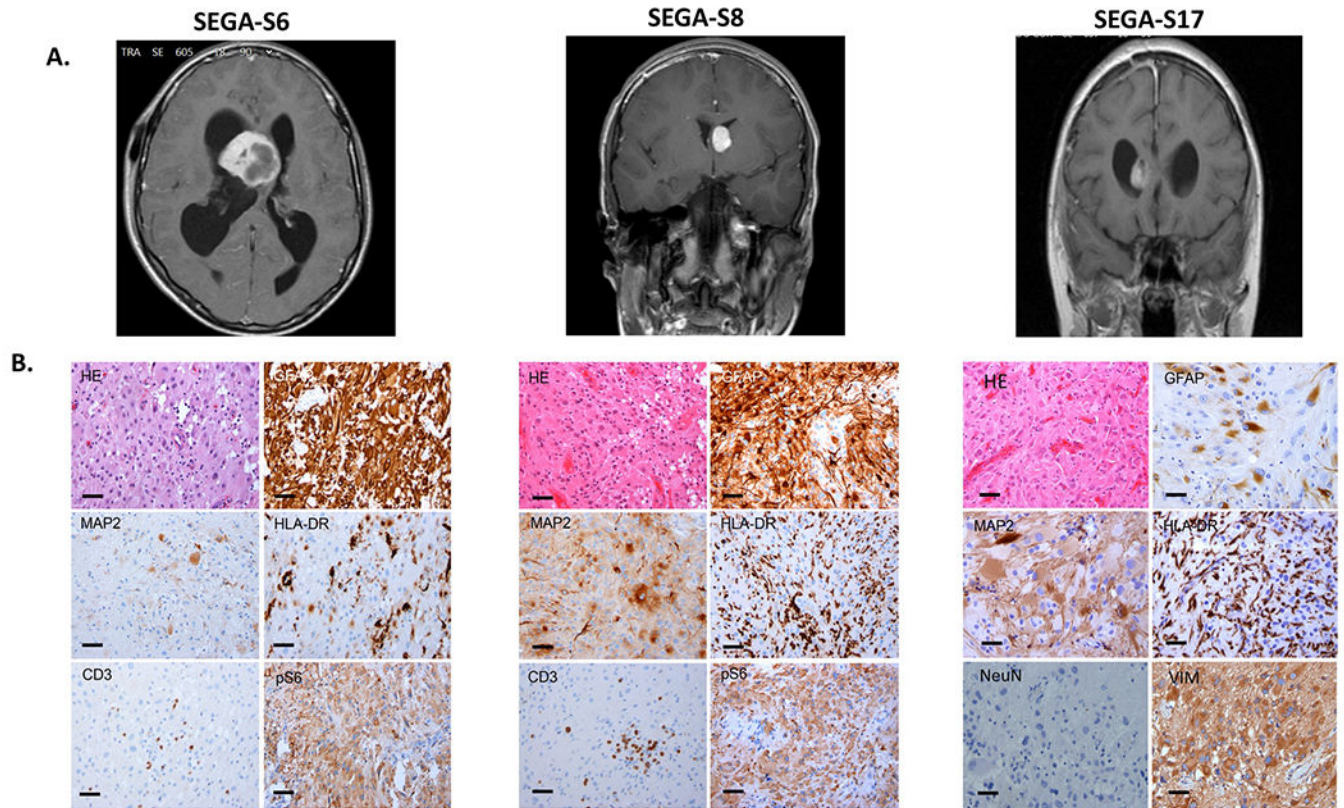


**Fig. 1: MRI images and histologic features of SEGAs.**

**a** T1-weighted coronal or sagittal gadolinium-enhanced MRI images showing SEGAs in the right lateral ventricle near the foramen of Monro (**SEGA-S6**, **SEGA-S17**), or in a similar location on the left (**SEGA-S8**) in 3 TSC subjects before surgical resection. **b** H&E and representative IHC images of the three corresponding SEGA tumors (**SEGA-S6**, **S8**, **S17**). H&E staining shows classical histological SEGA features, with giant cells in a mixed glial background with blood vessels. Variable expression of the glial marker GFAP is seen, with diffuse immunoreactivity in 2 of 3 samples shown here, with less staining for MAP2. HLA-DR staining highlights variable numbers of microglial cells, and CD3 staining shows presence of scant intratumor T lymphocytes; Variable expression of the neuronal marker MAP2 is seen. IHC is negative for the neuronal nuclear marker NeuN, but positive for intermediate filament vimentin (**SEGA-S17**). Activation of mTORC1 in tumor giant cells is indicated by expression of pS6. Scale bars: 100 μm.

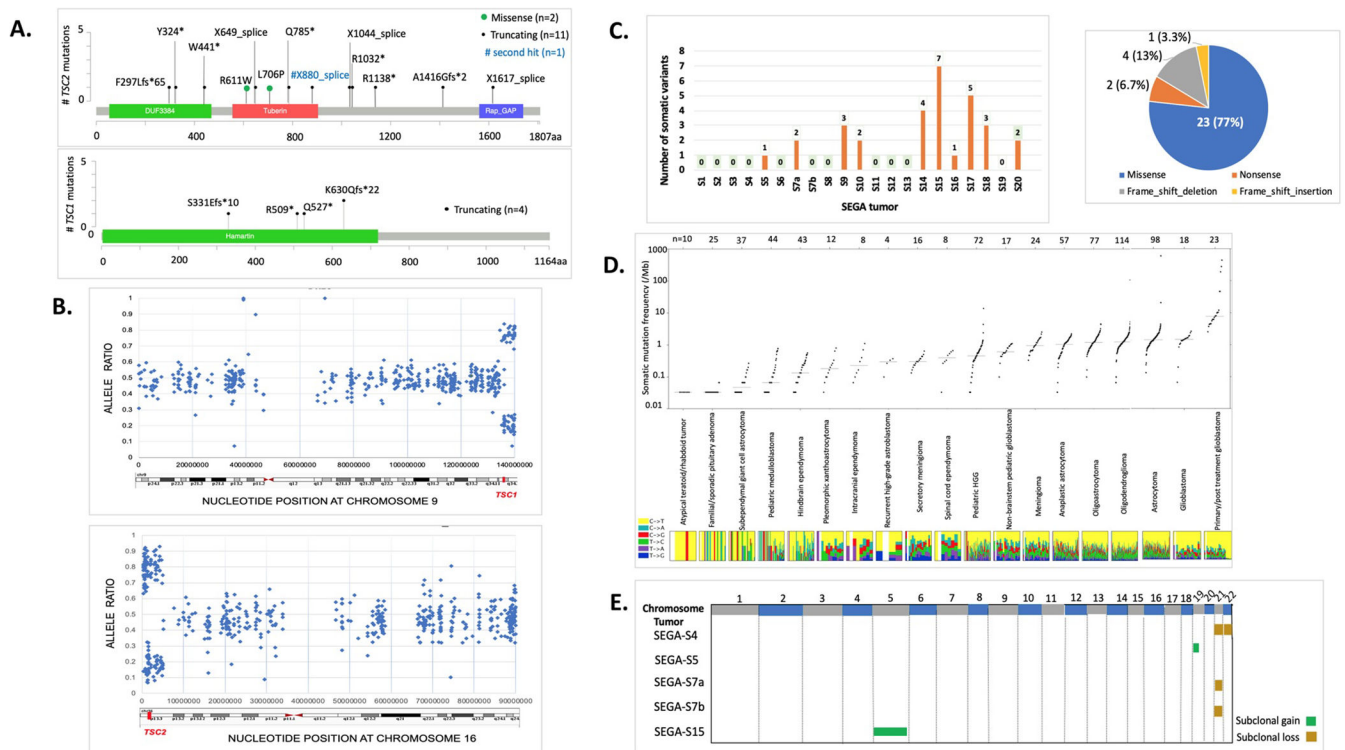


**Fig. 2: Germline and somatic alterations in SEGAs.**

**a** Position and type of germline and somatic *TSC1/TSC2* pathogenic variants in 19 SEGAs.

**b** Examples of Copy Neutral Loss of Heterozygosity (CN-LOH) in two representative SEGAs (**SEGA-S9** and **S13**), encompassing chr9:134,398,493–141,070,719 (6.7 Mb, top) and chr16:304,514–4,942,099 (4.64 Mb, bottom) (GRCh37/hg19). SNP allele frequency (AF) distribution is shown across the entire chromosome with regions of AF skewed from the expected 0.5 (range: 0.4–0.6) in regions surrounding *TSC1* (top) or *TSC2* (bottom). Each blue dot depicts a single SNV. **c** Number and type of small somatic variants in 21 SEGAs. **d** Somatic mutation frequency per Mb in SEGAs in comparison to a broad range of pediatric and adult brain tumors. Each dot in the plot represents a different tumor. *Y* axis is log scale. **e** Five of 21 (19%) SEGAs harbor subclonal chromosomal copy number gain (green) or loss (brown).



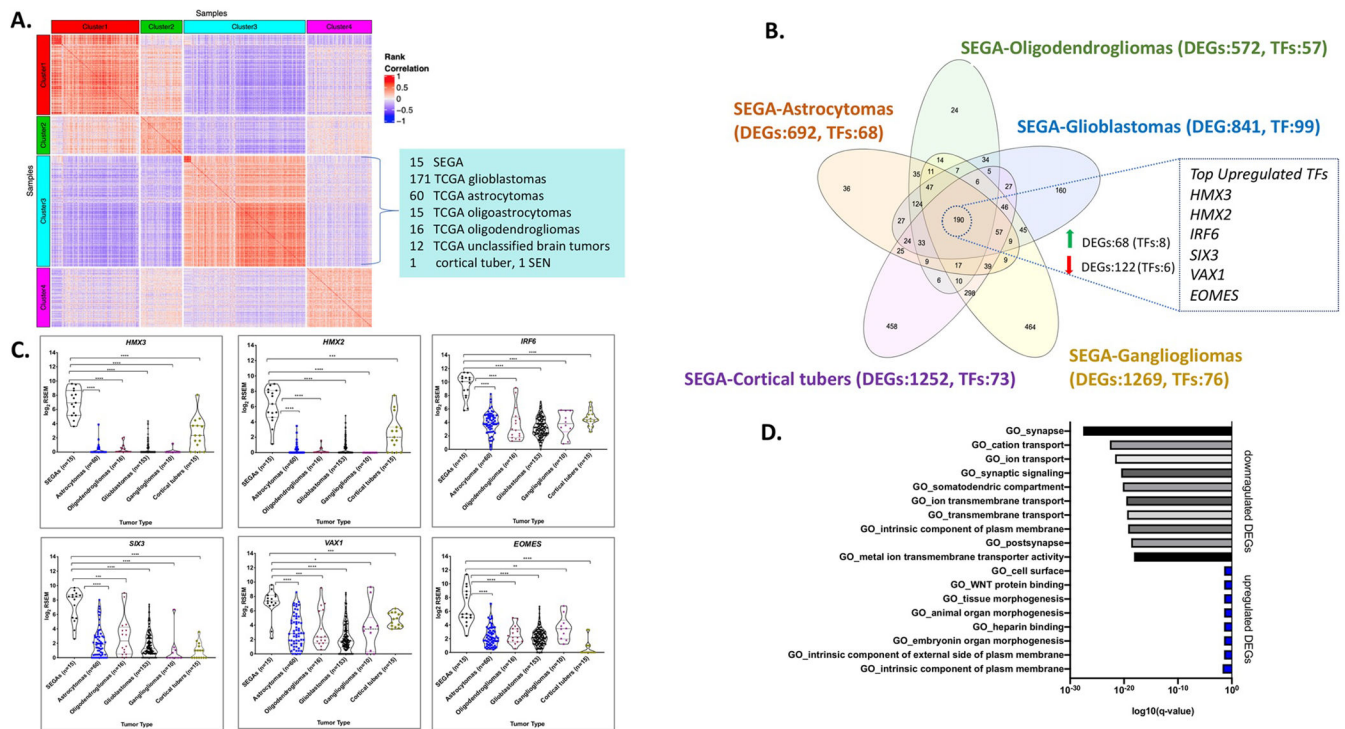


**Fig. 3: Comparison of RNA-Seq expression of SEGAs to other brain tumors and cortical tubers.**  
**a** A heatmap is shown reflecting a *de novo* clustering analysis using 3060 most variable genes in the combined cohort of: SEGAs ( $n = 16$ ), TCGA LGG ( $n = 530$ ), TCGA GBM ( $n = 171$ ), cortical tubers ( $n = 15$ ), SEN samples ( $n = 2$ ), and normal brain samples ( $n = 11$ ). Pairwise sample by sample Spearman rank correlation was determined and used to generate the heatmap that is shown. Fifteen of 16 (96%) SEGAs are in Cluster 3, form the red square in the upper left corner of Cluster 3, reflecting a high rank correlation among them. Cluster 3 also contains most GBM ( $n = 163$ ) and a subset of TCGA LGG ( $n = 103$ ). **b** Venn diagram of all DEGs (FDR < 0.05) in SEGAs versus each of five other histological subtypes of brain tumors/cortical tubers. Notably, a set of 190 genes were differentially expressed in SEGAs compared to each of the other five sample types. The TFs that are upregulated in SEGAs are shown at right. **c** Violin dot plots of the top 6 TFs that were differentially and highly expressed in SEGAs compared to other brain tumors and cortical tubers. **d** GO pathways showing enrichment for the 190 DEGs: top, pathways enriched in genes downregulated in SEGA; bottom, pathways enriched in genes upregulated in SEGA.

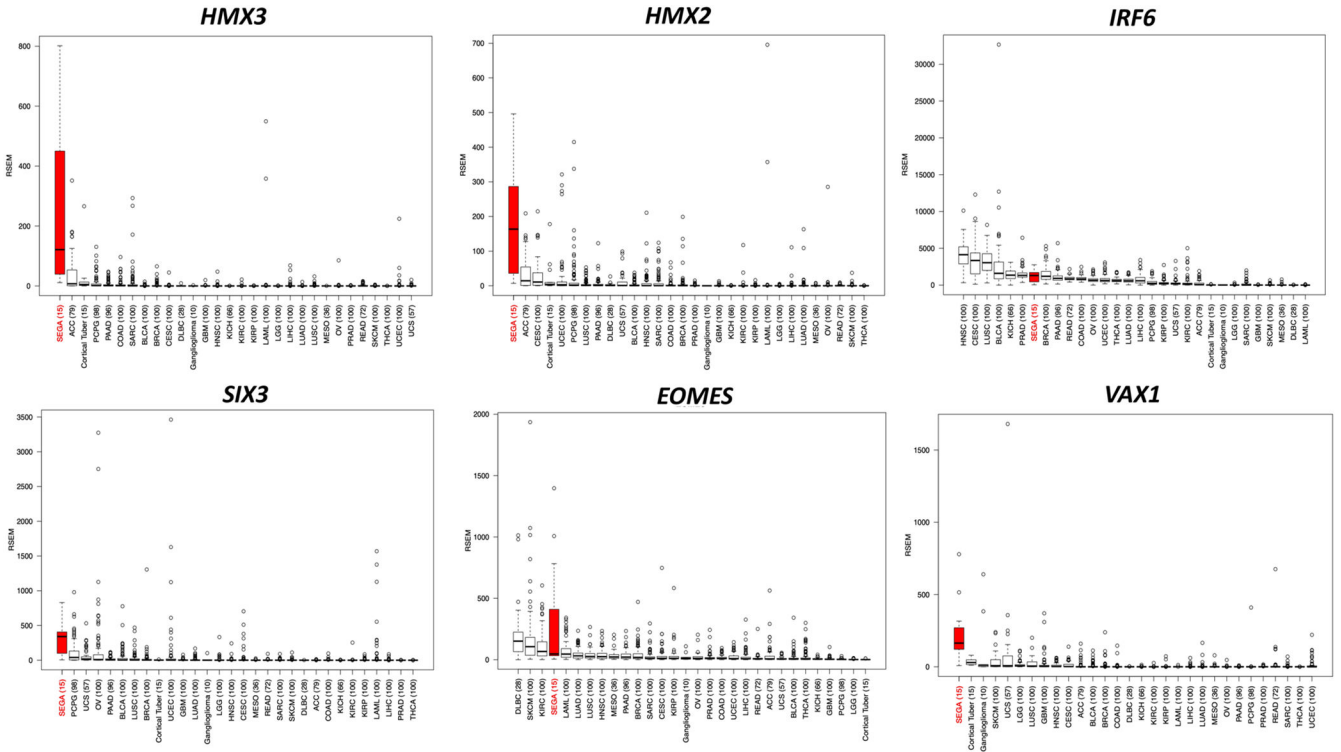


**Fig. 4:** Box plots for the top six DE (upregulated) TFs in SEGA compared to TCGA tumors (2463 tumors of 27 different histologic types), gangliogliomas and cortical tubers. Abbreviations for all TCGA tumor types at: <https://gdc.cancer.gov/resources-tcga-users/tcga-code-tables/tcga-study-abbreviations>. Gene expression is shown in RSEM values.

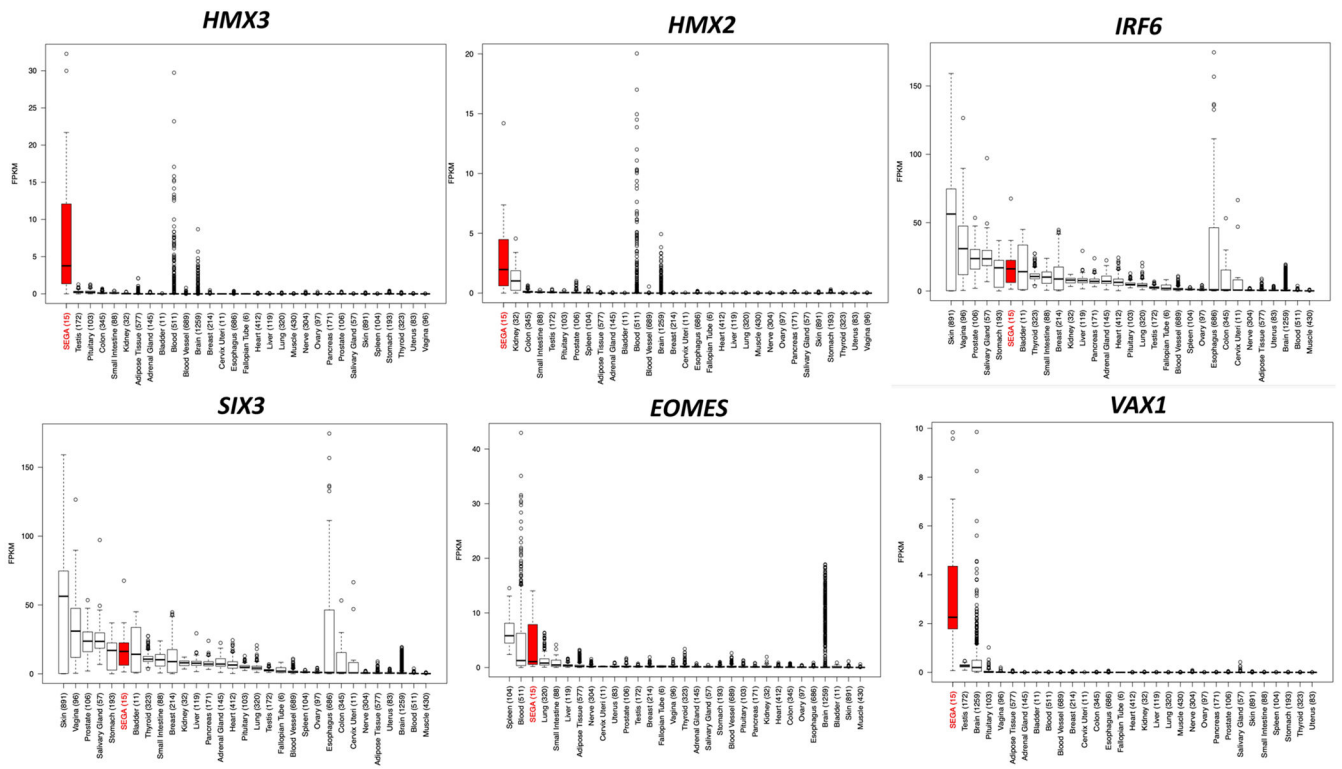


**Fig. 5:** Box plots for the top six DE (upregulated) TFs in SEGA compared to GTEx human normal tissues (~8500 samples from 30 normal tissue types, v6p release). Gene expression is shown in FPKM values.

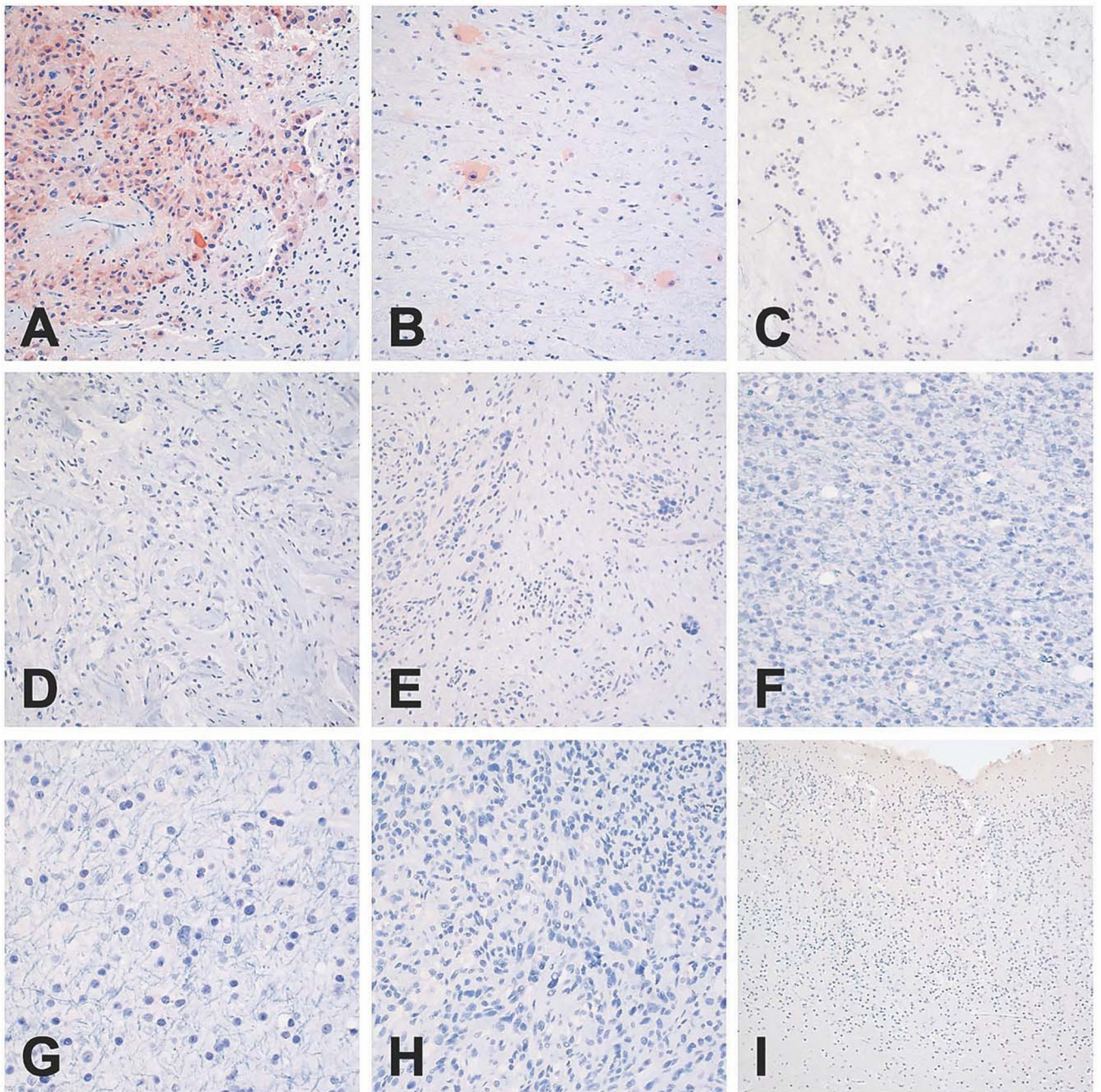


**Fig. 6: Representative images of IRF6 immunohistochemistry.**

Cytoplasmic staining was observed only in SEGAs (a) and in the balloon neurons of cortical tubers (b). No cytoplasmic immunoreactivity was noted in subependymomas (c), gangliogliomas (d), PXAs (e), oligodendrogliomas (f), astrocytomas (g), glioblastomas (h), or in normal infant cortex (i). Scale bar: 400  $\mu$ m, PXA: Pleomorphic xanthoastrocytoma.

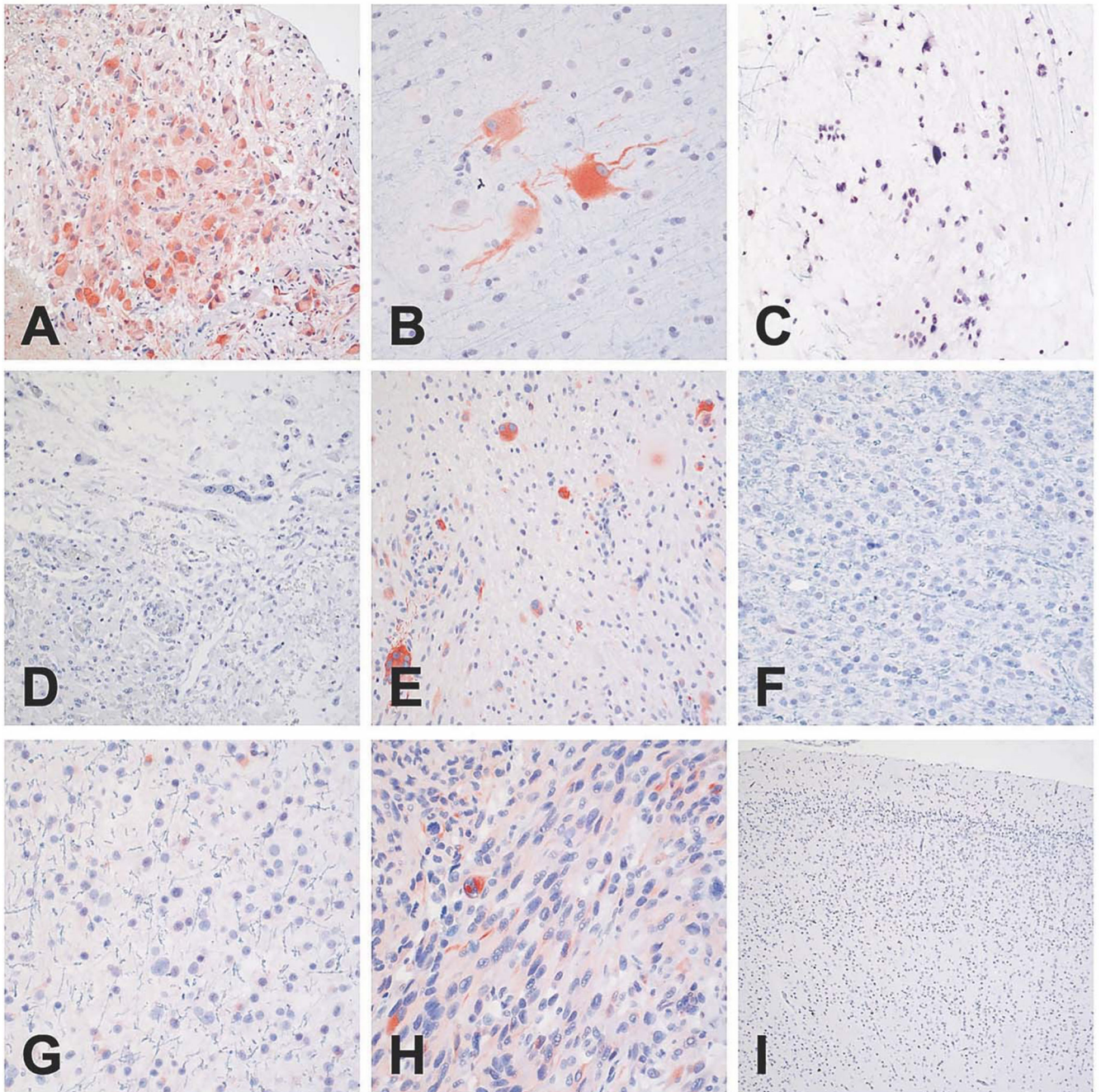


**Fig. 7: Representative images of SIX3 immunohistochemistry.**

Strong and diffuse cytoplasmic staining was predominantly limited to SEGAs (a) and in the balloon neurons of cortical tubers (b); however, occasional examples of PXA showed positive staining in large pleomorphic tumor cells (e). Glioblastomas exhibited staining in scattered cells (h). No cytoplasmic immunoreactivity was noted in subependymomas (c), gangliogliomas (d), oligodendrogliomas (f), astrocytomas (g), or in normal infant cortex (i). Scale bar: 400  $\mu$ m, PXA: Pleomorphic xanthoastrocytoma.

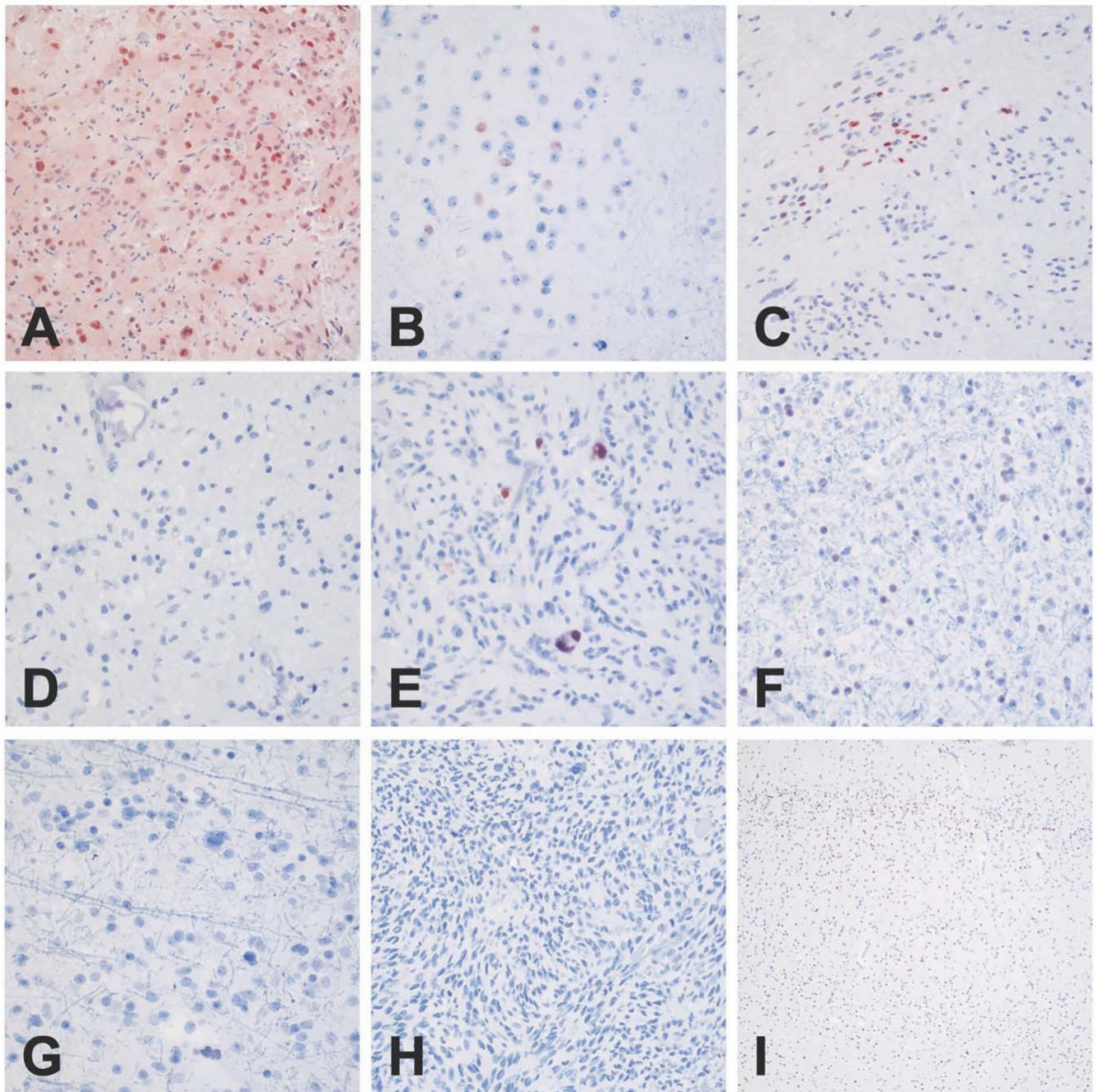


**Fig. 8: Representative images of VAX1 immunohistochemistry.**

Nuclear staining was observed in all SEGAs (a) and focal staining was seen in abnormal clusters of neurons, consistent with balloon neurons in cortical tubers (b). Occasional examples of subependymoma displayed focal nuclear positivity (c), and a single PXA showed positive staining in large pleomorphic tumor cells (e). No nuclear immunoreactivity was noted in gangliogliomas (d), oligodendrogliomas (f), astrocytomas (g), glioblastomas (h), or in normal infant cortex (i). Scale bar: 400  $\mu$ m, PXA: Pleomorphic xanthoastrocytoma.

Table 1

Clinicopathological data for 20 TSC patients with 21 resected SEGA tumors.

Subject	Age (at surgery)-years	Gender	Tumor location	Tumor size (cm)	Treatment prior to surgery	Treatment	Epilepsy	Age at onset epilepsy	Seizure frequency prior to surgery	Other clinical manifestations
SEGA-S1	1	M	Right lateral ventricle	3 × 3	Yes	Antiepileptic/sirolimus (non-responder)	Yes (drug-resistance)	1 month	Daily	Cortical tubers
SEGA-S2	2	M	Left ventricle	2.5 × 3.5 × 3	Yes	Antiepileptic	Yes (severe)	1 month	Daily	Cortical tubers, PKD, cystic tubers, autism, severe ID, renal insufficiency
SEGA-S3	6	M	Right ventricle	6 × 4.4 × 4.5	Yes	Antiepileptic	Yes	2 months	2–3/week	Cortical tubers, cardiac rhabdomyoma, FA, ID, autism, hydrocephalus, vomiting, vision loss
SEGA-S4	9	M	Left lateral ventricle	2 × 1.5 × 0.4	Yes	Antiepileptic	Yes (with complex partial seizures)	15 months	Weekly/biweekly subtle seizures	Bicuspid aortic valve, right FR cortical tuber and right TL subcortical tuber
SEGA-S5	9	M	Right ventricle (foramen Monro)	1.2 × 1.2 × 1.4	Yes	Topical rapamycin 1% ointment for facial lesions	No	N/A	N/A	Cortical tubers, HMM, FA, peritumoral fibromas, SENS, renal AMLs, above average intellect
SEGA-S6	14	M	Intraventricular, cerebrum	4	Yes	Antiepileptic	Yes	4 years	N/A	Cortical tubers, kidney AML, visual loss, normal intellect
SEGA-S7	14	M	Two SEGAs, one in right and one in left ventricle	RV: 3.5 × 2 × 2.5, LV: 2.5 × 1.5 × 0.8	No	N/A	No	N/A	N/A	Cortical tubers, mild FA, normal intellect, acute hydrocephalus
SEGA-S8	15	M	Left ventricle	1.5	Yes	Antiepileptic	Yes	10 years	Daily nondisabling (5–6 per day)	Cortical tubers, kidney AML, normal intellect
SEGA-S9	17	M	Right ventricle (foramen Monro)	3.5 × 3 × 2.5	No	N/A	No	N/A	N/A	History of morning headache and vomiting (raised ICP symptoms related to hydrocephalus), mild ID
SEGA-S10	23	M	Ventricle (foramen Monro)	N/A	Yes	Antiepileptic	Yes	3 years	2–3 per 6 months	Cortical tubers, kidney AML, normal intellect
SEGA-S11	1	F	Right lateral ventricle	3 × 3	Yes	Antiepileptic	Yes	1 month	Daily	Cortical tubers
SEGA-S12	6	F	Left lateral ventricle	6 × 5 × 2	Yes	Antiepileptic	Yes (drug-resistance)	3 days	Daily seizures	Cortical tubers, severe TSC presentation: cortical dysplasia (surgery at age 1), FA, kidney AML, cardiac rhabdomyoma,

Author Manuscript

Author Manuscript

Author Manuscript

Author Manuscript

Subject	Age (at surgery)- years	Gender	Tumor location	Tumor size (cm)	Treatment prior to surgery	Treatment	Epilepsy	Age at onset epilepsy	Seizure frequency prior to surgery	Other clinical manifestations
SEGA-S13	11	F	Frontal horn of right lateral ventricle	2.4 × 1.7 × 2.3	No	N/A	No	N/A	N/A	severe ID, autism, acute hydrocephalus Cortical and subcortical tubers, subependymal nodules, FA, shagreen patch, hypomelanotic macules, renal angiomyolipomas, retinal hamartomas, normal development, complaints of blurry vision and some nausea
SEGA-S14	13	F	Left lateral ventricle	4 × 3	Yes	Antiepileptic	Yes	17 months	N/A	Cortical tubers
SEGA-S15	13	F	Right ventricle	1 × 2 × 3	Yes	Antiepileptic	Yes	9 months	No seizures for >2 years	Cortical tubers, FA, kidney AML
SEGA-S16	14	F	Right ventricle	3.5 × 2.5 × 0.8	Yes	Antiepileptic	Yes	12 months	No seizures for >2 years	Cortical tubers, kidney AML, FA, hydrocephalus, vision loss
SEGA-S17	14	F	Intraventricular	N/A	No	N/A	No	N/A	N/A	Cortical tubers, kidney AML, normal intellect
SEGA-S18	22	F	Left lateral ventricle	3.5 × 1.5 × 0.6	Yes	Antiepileptic	Yes (intractable)	N/A	N/A	Cortical tuber, hydrocephalus, fibroadenoma of right breast, hydrocephalus, malignant neoplasm of cerebrium, except lobes and ventricles
SEGA-S19	47	F	Right frontal	1.5 × 0.8 × 0.2	No	No	No	no	no	FA, SEN, kidney AML, renal cysts, 3 healthy offspring
SEGA-S20	17	F	Right lateral ventricle	1.0 × 0.8 × 0.7	No	N/A	Yes	0	Uncertain	Cortical tubers, ASD, cognitive impairment, behavioral issues, renal AMLs, FA, oral fibromas

I. M male, F female, PKD polycystic kidney disease, AML angiomyolipoma, ID intellectual disability, ASD autism spectrum disorder, HMM hypomelanotic macules, FA facial angiofibroma, SEN subependymal nodule, RV right ventricle, LV left ventricle, ICP Increased Intracranial Pressure.



Table 2

List of the top 44 upregulated DEGs, common to all pairwise comparisons between SEGAs and other brain tumors/cortical tubers, with a median fold change  $\geq 10$  and FDR/ $q$ -value  $< 0.05$ .

Gene ID	SEGAs to TCGA astrocytomas		SEGAs to TCGA oligodendrogliomas		SEGAs to TCGA glioblastomas		SEGAs to gangliogliomas		SEGAs to cortical tubers		Median fold change
	Fold change	Fold change	Fold change	Fold change	Fold change	Fold change	Fold change	Fold change	Fold change	Fold change	
<i>HCRTR2</i>	253.2	239.6	309.5	309.5	154.7	34.9	239.6				239.6
<i>SFTA3</i>	168.1	152.6	196.7	196.7	203.5	106.3	168.1				168.1
<i>SPAN8</i>	141.8	148.4	324.7	324.7	240.7	77.1	148.4				148.4
<i>KCNK12</i>	130.3	164.3	195.4	195.4	36.0	11.7	130.3				130.3
<i>LHCGR</i>	111.7	85.1	102.5	102.5	14.7	60.7	85.1				85.1
<i>SLN</i>	81.0	125.1	46.2	46.2	1082.1	39.3	81.0				81.0
<i>HMX3</i>	79.8	70.2	76.5	76.5	88.9	17.5	76.5				76.5
<i>HMX2</i>	51.1	55.0	58.1	58.1	83.5	14.9	55.0				55.0
<i>SLC14A2</i>	39.3	35.1	55.2	55.2	53.8	86.2	53.8				53.8
<i>FRZB</i>	69.6	48.1	41.1	41.1	47.0	11.7	47.0				47.0
<i>IRF6</i>	37.2	44.8	71.1	71.1	50.9	28.2	44.8				44.8
<i>SIX3</i>	30.3	18.1	43.0	43.0	71.1	75.5	43.0				43.0
<i>TMPRSS2</i>	29.3	25.2	41.9	41.9	116.8	57.3	41.9				41.9
<i>TRIM63</i>	35.4	52.2	32.2	32.2	35.8	7.1	35.4				35.4
<i>TRDN</i>	35.3	44.5	63.8	63.8	11.0	6.9	35.3				35.3
<i>GPNNMB</i>	35.3	31.2	31.5	31.5	77.0	19.9	31.5				31.5
<i>LOC148145</i>	14.9	29.7	38.0	38.0	66.4	6.0	29.7				29.7
<i>HGD</i>	30.3	25.9	11.1	11.1	25.2	4.3	25.2				25.2
<i>SLC39A2</i>	24.1	30.5	16.7	16.7	30.3	11.0	24.1				24.1
<i>FOLR1</i>	18.5	13.5	18.1	18.1	162.6	56.1	18.5				18.5
<i>SFRP1</i>	18.3	18.6	33.9	33.9	18.0	8.1	18.3				18.3
<i>ITIH1</i>	18.1	18.3	9.0	9.0	26.6	10.0	18.1				18.1
<i>TDGFI</i>	17.9	30.8	43.6	43.6	15.1	7.7	17.9				17.9
<i>LRRN4CL</i>	8.9	22.9	7.2	7.2	39.5	16.2	16.2				16.2
<i>LGR5</i>	16.0	18.3	30.7	30.7	9.8	10.3	16.0				16.0
<i>EOMES</i>	15.7	13.5	16.1	16.1	6.2	46.4	15.7				15.7

Gene ID	SEGAs to TCGA astrocytomas		SEGAs to TCGA oligodendrogliomas		SEGAs to TCGA glioblastomas		SEGAs to gangliogliomas		SEGAs to cortical tubers		Median fold change
	Fold change		Fold change		Fold change		Fold change		Fold change		
<i>GSTAI1</i>	16.1	18.6			13.9		15.4		8.5		15.4
<i>SFRP4</i>	8.9	11.4			16.6		15.0		31.0		15.0
<i>WISP2</i>	14.8	14.9			19.4		28.8		7.7		14.9
<i>GPRC5A</i>	16.8	11.6			11.7		47.4		14.7		14.7
<i>HKDC1</i>	17.6	11.0			21.5		14.7		10.6		14.7
<i>GALNT5</i>	11.4	14.6			12.6		16.7		61.9		14.6
<i>SYPL2</i>	10.6	15.8			13.7		16.7		8.5		13.7
<i>TNNC1</i>	13.4	14.6			9.3		16.6		8.2		13.4
<i>KCP</i>	13.2	11.7			10.9		15.5		12.9		12.9
<i>ELSPBP1</i>	12.8	10.9			7.6		14.2		13.2		12.8
<i>VAX1</i>	14.3	11.9			33.6		12.7		5.7		12.7
<i>FGFBP2</i>	9.7	12.6			8.4		81.9		31.4		12.6
<i>IP6K3</i>	8.7	12.5			9.6		13.8		16.4		12.5
<i>TMEM200A</i>	13.9	8.8			25.6		12.5		5.1		12.5
<i>TTC39A</i>	11.9	25.7			12.4		10.6		8.2		11.9
<i>GPR1</i>	20.7	11.1			6.3		18.5		8.6		11.1
<i>F10</i>	10.8	15.1			12.8		6.5		10.4		10.8
<i>HORMAD2</i>	10.2	10.9			10.0		5.5		4.3		10.0

*I*. Genes highlighted in bold are TFs.